




A Robotic Microscope System to Examine T Cell Receptor Acuity Against Tumor Neoantigens: A New Tool for Cancer Immunotherapy Research

Lee-Ling Sharon Ong , Hai Zhu, Debasis Banik, Zhenping Guan, Yinnian Feng, Ellis L. Reinherz , Matthew J. Lang, and H. Harry Asada 

Abstract—During immune surveillance, cytotoxic T lymphocytes (CTL) can selectively identify and destroy tumor cells by recognizing tumor-specific peptides (neoantigens), bound to major histocompatibility complex molecules (pMHC) arrayed on cancer cell surfaces. CTL use the same machinery to destroy virally infected cells displaying pathogen-specific pMHC, while leaving intact healthy cells expressing normal self-pMHC. We present a robotic microscope that allows scientists to conduct highly sensitive and selective T cell-pMHC studies with high throughput. Our system manipulates micro-meter beads coated with particular pMHC, presents them to T cells and generates piconewton-level intermolecular forces required to detect T cell acuity with a neoantigen. Our system integrates optical tweezers, precision nano-micro stages, and episcopic/diascopic illumination schemes at two magnifications. We create a coordinate referencing system to locate translucent T cells in three-dimensional, over a large space, based on the characteristic intensity change at each focal plane caused by the cells. Our system performs automated experiments to detect the level of T cell acuity with specific pMHCs, by measuring the downstream cellular responses. High acuity T cells can be selectively recovered for single cell analysis. Our new methodology and tool will have a significant impact on cancer immunotherapy and immunology research.

Index Terms—Automation at micro-nano scales, automation in life sciences, biotechnology, pharmaceutical and health care, biological cell manipulation.

I. INTRODUCTION

IMMUNOTHERAPY is an active research area in cancer treatment aimed at harnessing the specificity and selectivity of T cells either through active patient vaccination to induce relevant cytotoxic T lymphocytes (CTL) or by adoptive (passive) transfer of those CTL into the cancer patient to destroy the tumor [1], [2]. Cancer immunotherapy exploits our body's natural defenses to treat cancer. Immune cells can distinguish specific antigens of tumor cells from self and the myriad of other antigens with extremely high sensitivity and selectivity. Cancer-specific T cells, for example, have T cell receptors (TCRs) that bind to tumor-related peptides (i.e. neoantigens) in the groove of major histocompatibility complex molecules arrayed on the surface of antigen presenting cells (APCs) [3]. Once bound to the TCR, an intracellular signalling cascade is triggered so that T cells proliferate and differentiate into effector cells or else memory T cells, the latter cells retain the immunological experience and are capable of detecting and killing tumor cells having the same peptide neoantigens in future encounters [3]. Adoptive transfer of these pMHC-specific T cells also offers an important avenue of immunotherapy. High acuity T cells are those whose TCRs can detect and discriminate a handful of “foreign” (i.e. non-self) peptide antigens amongst a sea of 100,000 normal self peptides and then initiate T cell activation.

A. T Cell-pMHC Studies

It is amazing that T cells are endowed with extremely high sensitivity and selectivity. Detailed mechanisms of selective detection and downstream response are still poorly understood, yet engaging such mechanisms in a manner physically similar to T cells undergoing surveillance is the key to successful immunotherapy [2], [3]. T cell-pMHC studies are generally performed with force free methods such as flow cytometry, live cell fluorescence microscopy, and elispot. Methods that apply force include optical tweezers, micropipettes, deformable surfaces and other force probes, a number of which are detailed in [4].

Manuscript received September 10, 2018; accepted January 3, 2019. Date of publication January 21, 2019; date of current version February 21, 2019. This letter was recommended for publication by Associate Editor S. C. Ryu and Editor Y. Choi upon evaluation of the reviewers' comments. This work was supported in part by the National Research Foundation, Singapore, through SMART Centre's BioSyM IRG research programme, in part by the NIH/NIAID under Grant R56AI138489, and in part by the National Science Foundation Science and Technology Center for Emergent Behaviors of Integrated Cellular Systems (CBET-0939511). (Corresponding author: Lee-Ling Sharon Ong.)

L.-L. S. Ong, H. Zhu, D. Banik, and Z. Guan are with the Singapore-MIT Alliance for Research and Technology, Singapore 138602 (e-mail: sharon.ong@smart.mit.edu; zhuhai@smart.mit.edu; debasis@smart.mit.edu; zhenping@smart.mit.edu).

Y. Feng is with the Department of Chemical and Biomolecular Engineering, Vanderbilt University, Nashville, TN 37235 USA (e-mail: yfeng86@stanford.edu).

E. L. Reinherz is with the Department of Medical Oncology, Laboratory of Immunobiology, Dana-Farber Cancer Institute and Department of Medicine, Harvard Medical School, Boston, MA 02115 USA (e-mail: ellis_reinherz@dfci.harvard.edu).

M. J. Lang is with the Singapore-MIT Alliance for Research and Technology, Singapore 138602, and also with the Department of Chemical and Biomolecular Engineering and Department of Molecular Physiology and Biophysics, Vanderbilt University, Nashville, TN 37235 USA (e-mail: matt.lang@vanderbilt.edu).

H. H. Asada is with the Singapore-MIT Alliance for Research and Technology, Singapore 138602, and also with the Department of Mechanical Engineering, Massachusetts Institute of Technology, Cambridge, MA 02139 USA (e-mail: asada@mit.edu).

Digital Object Identifier 10.1109/LRA.2019.2894466

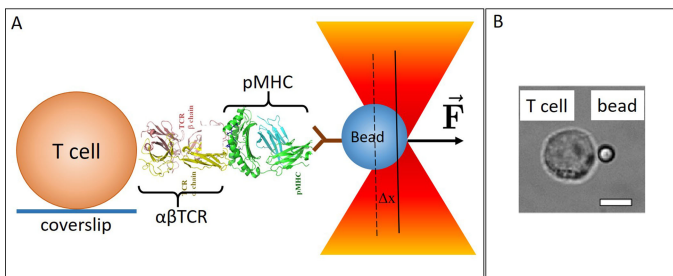


Fig. 1. (A) Cartoon illustration of the bead-cell contact interface. The optical tweezers control bead position to actively present pMHC molecules to a T cell immobilized on a glass surface. The trap applies pN forces on the T cell through the bead-cell interface. If the T cell's mechanosensing apparatus is engaged, the bead will be displaced out of the center of the trap (denoted by Δx) and downstream cellular responses will be generated. The latter can be measured as a change in the T cell fluorescence reporting on intracellular calcium. (A) does not represent the location of the trap and true scale of the objects. In practice, the trap is right next to the T cell (shown in (B)). Scale bar: $5 \mu\text{m}$.

Approaches such as flow cytometry and live cell microscopy work under equilibrium and typically require much higher pMHC concentrations than physiologically present to activate T cells. However, T cell activation is a non-equilibrium process. Although force based methods such as optical tweezers, micropipettes and other force probes are low in throughput, they are capable of working out of equilibrium where the TCR mechanosensor machinery is energized. The two dominant methods for measuring T cell sensitivity and selectivity are micropipettes and optical tweezers. While single molecule studies can be performed with both methods at piconewton (pN) forces, the optical tweezers is superior exhibiting nanometer position resolution (where conformation changes of the pMHC-TCR linkage have been observed [5]) and pN force resolution allowing controlled application of load magnitude and direction and the determination of critical equilibrium forces [6].

Optical tweezers confine microscopic particles in 3D, through forces exerted by the intensity gradients of a strongly focused laser. This force is proportional to the displacement of the bead from the center of the trap. The trapping is due to the transfer of photon momentum to a particle with a refractive index slightly higher than the surrounding medium. In these studies, optical tweezers are used to manipulate micro-meter sized beads coated with target pMHC molecules. These tweezers can control the relative motion between the bead and a T cell, which is fixed to a coverslip surface [7], [8]. As shown in cartoon in Fig. 1, an antigen in the native form of a pMHC molecule is presented to a T cell where the relative bead location is controlled so that a pN-level intermolecular force may be generated.

Although optical tweezers deliver significant photon flux to the bead, we chose an infrared wavelength laser (1064 nm) that minimizes cell and protein damage. Bead placement at the side of the cell along the mid-line ensures that most of the trap photons do not interact with the cell. Heating is also minimal or non-existent. Given the exquisite control over force magnitude, we can apply forces to engage mechanosensor machinery without causing disruptive protein unfolding. Such force, applied through a step jump, is only sustained by the proteins for a brief period as the system relaxes in a few seconds to the triggering

as described [8]. The pulling geometry and force magnitudes are easy to control with optical traps making this method ideal for force-based T cell activation studies.

These optical tweezers studies entail fine (nano-meter scale) positioning accuracy, tiny (pN scale) directionally applied force and a number of manually performed steps including loading the sample, finding a cell, finding a bead, calibrating a bead and measuring the cell response. Manual operations are inaccurate and time consuming and require an expert operator. Furthermore, manual operations also introduce more chances for sample contamination. Here, we present a new robotic microscopy system for immunotherapy research to improve the throughput and accuracy of these studies, permitting the tasks to be performed remotely in a sterile environment. We aim to measure the downstream cellular response of T cells when they are actively interacting with specific antigens.

B. Related Work and Challenges

Many robotic systems have been developed for applications in single cell manipulation. These systems include automated magnetic tweezers to measure cytoplasm viscosity [9] as well as automated micro-pipettes to aspirate cells [10], [11], deposit and pattern single cells [12] and measure cell morphologies [13]. Various automated optical tweezers techniques have been reported, ranging from applications to manipulate a single microscopic bead [14], [15] to multiple objects simultaneously [16], [17], including cells [18], [19]. In addition to that, magnetic microrobotic systems [20] and automated lab-on-chip devices [21] have been developed for targeted protein binding and detection. To our knowledge, there are no other robotic systems to manipulate T cells to interact with pMHCs.

There are significant technical challenges in our methodology. The non-equilibrium force based binding acuity test described previously needs nanometer-scale precise positioning and precise force application. While the test must be performed for each cell one by one, the entire operation must be completed before cellular environmental conditions deteriorate. Therefore, high throughput is desirable. Furthermore, finding and viewing cells themselves is challenging because of cell transparency, low scattering and poor contrast within a given field of view (FOV). The sample contrast varies depending on the focal plane and hence it is a challenge to find the optimal focal plane for cell detection. Binding acuity tests require high Numerical Aperture (NA) optics and magnification typically 100X with an oil immersion lens. At this magnification, the FOV is narrow (typically around $40 \mu\text{m}$ by $60 \mu\text{m}$). For these tests, the cells are sparsely distributed on a glass slide. Hence, the average separation between cells does not permit visualization of more than one cell with the 100X field of view. We must cover a wide FOV, while the accuracy/resolution required for the avidity test is very high and it is impractical to switch microscope nosepieces with an oil immersion lens.

To address these issues, we developed a customized, automated system integrating bright field microscopy hardware, fluorescence detection, image analysis software, optical tweezers, and a sub-nanometer resolution stage. We built a microscopy system with episcopic and diascopic illumination schemes.

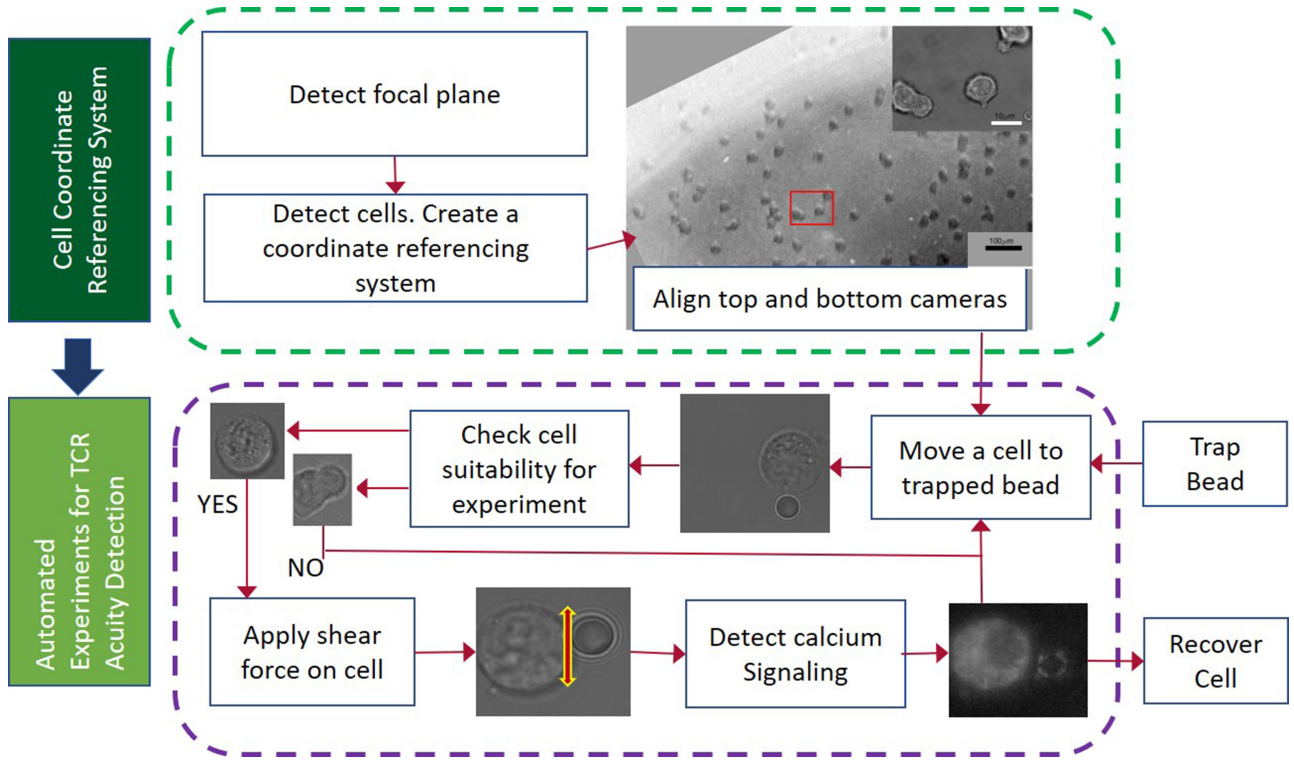


Fig. 2. Operation workflow diagram. Firstly, we create a referencing system of all the cell coordinates with images acquired from the top camera. Next, we locate the FOV of the 100X (indicated by the red rectangle) within the 20X image (black scale bar: $100\ \mu\text{m}$, white scale bar: $10\ \mu\text{m}$). A bead is detected and trapped with optical tweezers. We then present each cell to the bead by moving the stage and check if the cell is suitable for experimentation. Shear force is exerted on the cell by moving the piezostage in the vertical direction. An increase in calcium signalling, which is detected by a photodiode, indicates that binding interactions have occurred. Cells with strong binding interactions can be recovered for single cell analysis.

Reflected and transmitted light images of the specimen are captured at two different magnifications, 20X and 100X. With the acquired images at 20X, we create a coordinate referencing system to locate all T cells.

With our referencing system, we efficiently position each T cell in the 100X FOV for physical activation with a pMHC-coated bead to study the downstream cellular responses. Our system controls two automatic stages at two different resolutions, one to position the cell to a bead at micrometer resolution and the second to move the cell at subnanometer resolution for binding tests with precise control over force application.

Our system substantially reduces times for finding beads, finding cells and performing calibrations. A significant time saver with our system is the coordinate mapping so that multiple desired cells can be recovered later. The optical layout with both 100X for trapping and 20X for the larger field of view permit these tasks on the same microscope. Currently recovery is performed on a second microscope where no more than 2-3 cells in a given field of view can be recovered. The downstream intent of this process is to a) sort out the cells based on acuity measurement of cell activation by specific pMHC and bioforces, b) recover cells separately between two bins of high and low acuity quality, and c) perform single cell (or a fewer number of cells) analysis. These include DNA and RNA analysis to identify TCR structures and transcriptomes that define the difference between the two groups. Furthermore, this method can be used for selecting high-quality T cells with high acuity that respond

through force to very low copy numbers of pMHC for expansion for T cell therapy.

Section II presents our experimental setup. Section III describes an image processing algorithm for coordinate referencing, while in Section IV, we present our image analysis solutions for automated T cell acuity testing.

II. SYSTEM OVERVIEW

A. Work Flow

This system for examining TCR quality comprises many steps of challenging procedures that must be conducted precisely in a limited time. Fig. 2 shows the overall work flow of the procedures; a) creating a referencing system of all the cell coordinates with images acquired from the top camera, b) positioning each cell to the limited FOV of the camera below, c) detecting and trapping a bead, and d) performing T cell acuity studies.

To study each cell individually, the cells are sparsely placed on a glass surface and are immobilized on it for force application. The top camera acquires images of broader views at a lower magnification. Techniques are developed to detect cells and create coordinate referencing system in the global XYZ frame for locating each cell. With these cell coordinates, we position each cell to the 100X FOV of the camera below. After focusing the cell in a local z-axis, we examine detailed cell morphology to evaluate if the cell is suitable for acuity studies.

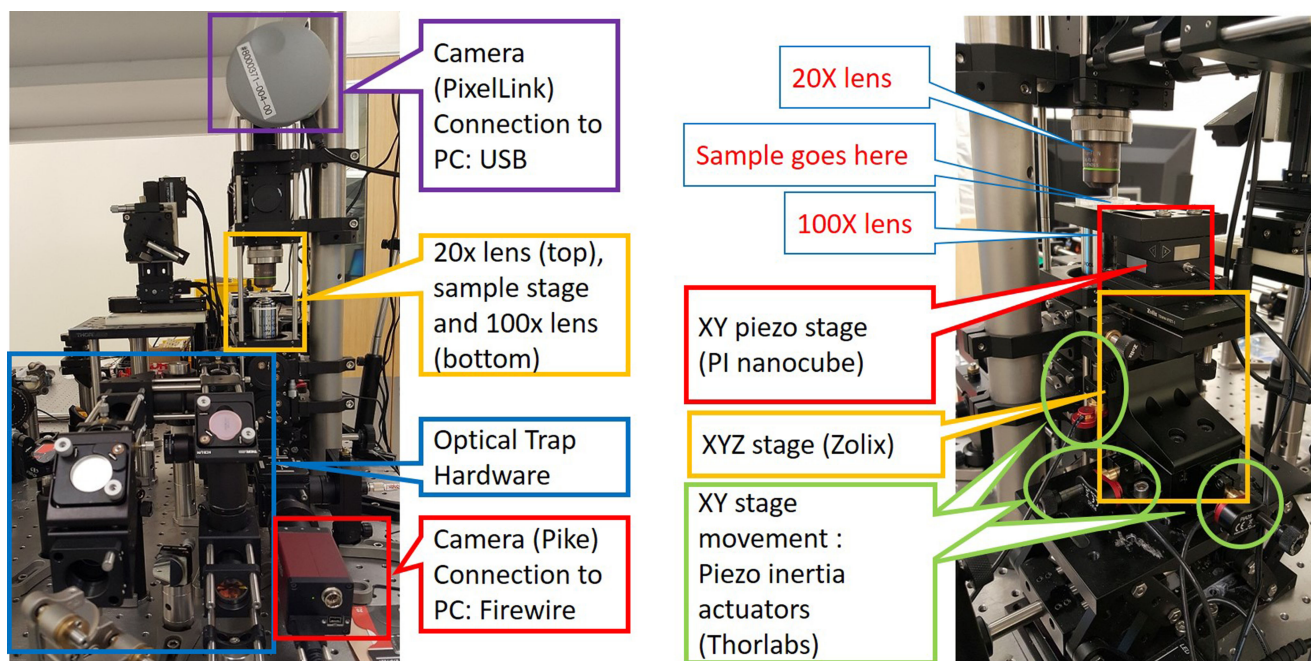


Fig. 3. The images acquired from above with a CCD Camera (Pixelink PL-B872CU), magnified with a Olympus UMPlanFI 20X objective and from below with another camera (Pike F-032B, Allied Vision Technologies) via a 100X magnification objective lens (Nikon, Plan Apo 100X). An infrared laser (Spectra Physics Excelsior-1064) is used for trapping. The sample is positioned by two motorized stages; a PI P-611.3 NanoCube stage allows sub-micron movements and a bearing linear XYZ stage (Zolix TM101) controlled via three piezo inertia actuators (Thorlabs PIA25).

For the selected cells the TCR acuity examination is performed. This requires precision manipulation, which is challenging and time-consuming. Our system automatically detects and captures a bead with optical tweezers, and then applies shear force to the cell with the trapped bead. The level of T cell acuity is then evaluated by measuring the calcium signaling levels through fluorescence detection.

B. Experimental Setup

Fig. 3 shows the overall view of the system. A collimated LED Lamp (Thorlabs, M530L3, 530 nm emission) is mounted above the specimen to provide transmitted light illumination. The main motivating factors for selecting transmitted light over fluorescence illumination as photobleaching and acquisition speed. Fluorescence imaging requires a pixel by pixel scanning to generate an image unlike transmitted light imaging.

Images are acquired from above with a CCD Camera (Pixelink PL-B872CU) magnified with an Olympus UMPlanFI 20X objective. Images are also acquired simultaneously with another camera (Pike F-032B, Allied Vision Technologies) via a 100X magnification objective lens (Nikon, Plan Apo 100X, 0.45 μm Depth of Field) below the specimen.

An infrared laser (Spectra Physics Excelsior-1064) is used for trapping beads. The cells are stained with a dye, which emits fluorescence signals when excited by another laser (Fibrotec Fiberoptics GMBH 488nm). The level of fluorescence, indicating the level of T cell avidity, is detected with an avalanche photodiode (APD). A multifunction data acquisition device (National Instruments USB v6229) controls the LED intensity, the 488nm laser intensity, and the shutter for the optical tweezers, and can detect the fluorescence level.

The sample is positioned by two motorized stages as shown in Fig. 3. A PI P-611.3 NanoCube stage allows for sub-micron movements with a limited range (250 μm). This stage is mounted on top of a long-stroke linear XYZ stage (Zolix TM101) with a 13 mm travel. This stage is controlled by a piezo inertia motor controller (Thorlabs TIM101) via three piezo inertia actuators (Thorlabs PIA25).

III. COORDINATE REFERENCING SYSTEM

Our goal is to detect the cells at 20X, create a grid referencing system, and move each cell to the 100X field of view for acuity studies. It is a challenge to detect the translucent cells or the optical focal plane in an efficient manner. Furthermore, the long-stroke stage is moved with piezo inertia actuators in open loop, where there could be over 20% of variation in the step size. As we move the stage to create a coordinate map, visual feedback is required to correct positioning errors.

A bright-field microscope typically comprises of a lamp, a condenser lens that focuses light from the source onto a specimen, an objective lens that collects light from the sample and magnifies the image, and a camera that captures the image of the specimen. By reducing the condenser aperture, the sample contrast can be enhanced [22].

If there is no specimen, the intensity distribution at the focal plane is uniform. However, if there is a specimen such as a biological cell, the intensity at the focal point alters due to reflected/transmitted light along the optical or z-axis. If the focal plane is inside the sample, there will be an area of higher intensity around the center of the cell, where the density of back-projected rays are higher.

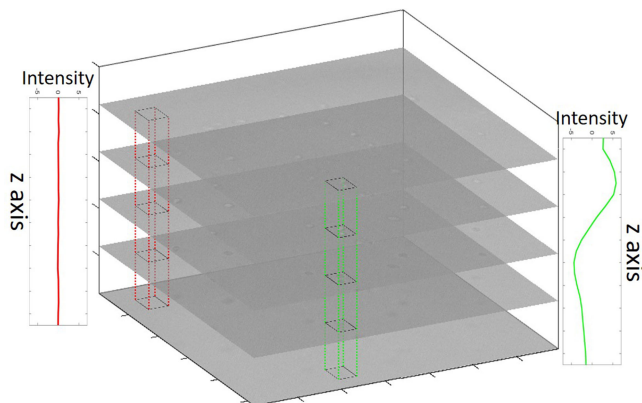


Fig. 4. Sample image of specimen at different focal planes along the z axis. The area bounded by the green lines contain two cells whereas there are no cells in the area bounded by the red lines. Cell appears brighter than the background when the focal point is slightly above or inside the specimen, and darker than the background when the focal point is below the specimen. The normalized change in mean intensity for both regions are shown by the red and green plot.

For focal planes under the specimen, the area immediately outside the cone of light formed by the specimen is completely dark due to the lack of back-projected rays [22]. The further away the focal plane is from the specimen, the lesser the contrast. Here, the cells appear more blurred and boundaries between cells which are close may merge.

We developed an approach to detect T cells in a large 3D space, capitalizing on these effects. The cell intensity changes at different focal points. The center of the cell appears brighter than the background when the focal point is slightly above or inside the specimen, and darker than the background when the focal plane is below the specimen. Although the cells are translucent [23], this intensity variation along the z-axis is significant and characteristic to the existence of a cell as shown in Fig. 4.

Hence, in order to detect the xy coordinates of the cell, we acquire images at multiple focal planes above and below the specimen, and compute the variance. By taking the standard deviation along the z-axis for every xy coordinate pixel, we obtain an image of the change in intensity distribution in the xy plane. By setting a threshold for this image, we can segment the x and y coordinates of each blob representing a cell or a number of cells.

Next, we locate the cells on the z-axis by selecting the best focal plane. At each acquired image stack, we find cell candidates by performing intensity thresholding to find a darker foreground, followed by size and solidity thresholding. We count the number of cells segmented at image stack and select the focal plane where we can reliably segment the most cells.

We then relate the 20X camera view to the 100X camera view to automatically bring each target cell within the 100X FOV. We initially fix an origin point within the 100X FOV, by manually selecting a cell in the 20X image and moving the table to view the cell within the FOV of the 100X camera. This cell location is defined to be the origin of coordinate axes. Next, the robotic system moves the stage automatically to each of the target cell based on the cells coordinates relative to the origin, to view other cells with the 100X camera.

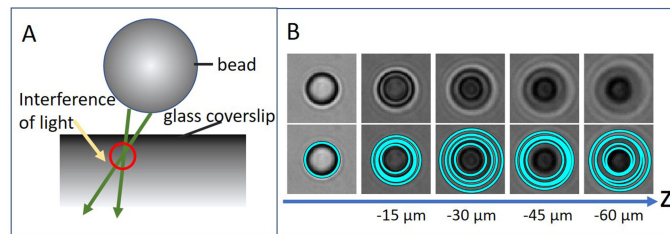


Fig. 5. (A) Illustration of image formation by Reflection Interference Contrast. The interference of light components back from the coverslip/buffer and the underside of the bead. The loci of interference (red circle) depends on the angle and divergence of incident light. (B) shows the pattern generated by a $3 \mu\text{m}$ bead as the distance between the bead and focal plane changes. This pattern, known as Newton rings, can be detected with circular Hough transforms. (bottom row in (B)) and determine the bead position on the z axis.

On the long range stage, there is a significant discrepancy between a commanded distance and the actual distance traveled. Due to the open loop nature of the inertia actuators and their prominent hysteresis, this “coarse” stage often slips and is unable to move the specimen correctly. Therefore, images cannot be indexed correctly based on the commanded distance given to the inertia actuators. We applied additional alignment techniques to align images as the stage moves in order to immediately detect and compensate for the slip. This solution allows us to build an accurate coordinate grid of cell locations with no significant performance degradation. In addition to the long-range stage, our system consists of a PIP-611.3 NanoCube stage for fine positioning accuracy.

IV. AUTOMATED EXPERIMENTS FOR TCR ACUITY DETECTION

During immune surveillance, T cells are activated when their surface $\alpha\beta$ T cell receptors (TCRs) recognize and mechanically interact with specific peptide ligands bound to MHC molecules (pMHCs) on APCs [3]. Mechanical force applied at the TCR-pMHC interacting interface elongates bond lifetimes for non-self-peptides (catch bonds) but shorten for self-peptides (slip bonds). The optimal force, crucial for T cell activation, is the force where T cell machinery is engaged or in other words the peak of the catch bond between the TCR and pMHC [8]. This force is typically around 15 pN.

Our goal is to activate as many cells as possible with the optical trap and then detect calcium flux change over time. It can be challenging to focus beads and locate them precisely against cells as there is drift along the optical axis. Furthermore, not all the cells are suitable for T cell acuity studies. Desirable cells for activation are circular and adhered to the surface.

A. Bead Detection and Holding

Optical tweezers use a lens to focus a collimated and normally incident laser beam to trap and manipulate particles in aqueous medium. For a bead to be successfully trapped, it has to be positioned in 3D near the beam focus by moving the stage in the XYZ direction. The interaction between the photons of a laser beam and the small bead to be trapped generates the trapping force. If a bead is too far below or above the focus of the laser, the trapping force would push the bead away.

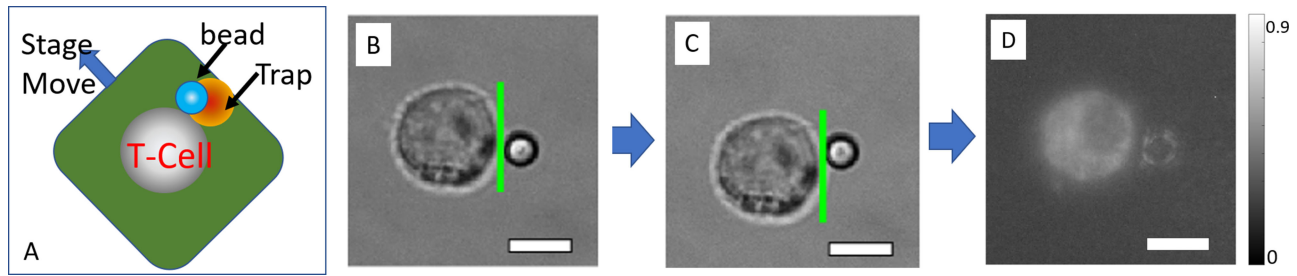


Fig. 6. (A) Cartoon showing optimal shear force directions of the bead relative to the cell. The trap is guided into contact with an immobilized T cell by moving the stage as shown in (B). A vectorial one-step force is applied to the bead by moving the piezoelectric stage to (C). The green line shows the edge of the cell detected via image analysis. The location of the edge is important in order to apply shear forces. The force along the T cell surface triggers a rise in free calcium signals. T cells were preloaded with calcium indicators, which could be visualized by a fluorescent imaging under 100X magnification (shown in D). We detect the calcium flux by an increase of fluorescence intensity in the cell. (Scale bar: 5 μm).

Our approach to 3D positioning of beads is based on Reflection Interference Contrast Microscopy (RICM). An RICM image is generated due to the interference of two reflected components of light; the incident light scattered from the underside of an object and the one from the coverslip/liquid interface as shown in Fig. 5(a). Spherical beads produce an interference pattern consisting of concentric Newton rings. This pattern changes as the bead position changes along the z axis, as shown in Fig. 5(b). By measuring these Newton rings, we can position the beads in the z-direction. Circular Hough transforms with multiple radii are used for detecting the Newton rings.

B. Controlled Application of Shear Force to Detect TCR Avidity

During immune surveillance, T cells attach to other cells, assuming a polarized morphology with a leading edge and lengthening uropod [7]. This action allows T cells to scan the cell surface to search and bind to specific foreign pMHCs such as antigenic peptides on cancer cells. The binding interaction between the TCR and pMHC can be magnified by the optimal force. The mechanical energy from this force is then converted into a biochemical signal, which elevates the intracellular free calcium in the cell [7].

Studies of TCR acuity are performed with T cells immobilized on poly-l-lysine coated glass coverslips and pMHC-bound beads [7]. By holding these beads with optical tweezers, we can control the direction and movement of each T cell relative to the bead by moving the piezoelectric stage. A directed movement tangential to the cell/bead interface (Figures 6(a) to (c)) generates pN shear forces. The example fluorescence intensity image of calcium flux in the cell, acquired with the 100X camera, is shown in Fig. 6(d).

Fig. 7 shows a T cell at different focal planes and the result of intensity thresholding at each plane. The top image shows the focal measure [24], defined as

$$\begin{aligned}
 FM(\sigma) &= \frac{1}{NM} \sum_{u,v} [f(u,v) \times G_u(u,v,\sigma)]^2 \\
 &\quad + [f(u,v) \times G_v(u,v,\sigma)]^2 \\
 &= \frac{1}{NM} \sum_{u,v} [f_u^2 + f_v^2]
 \end{aligned} \quad (1)$$

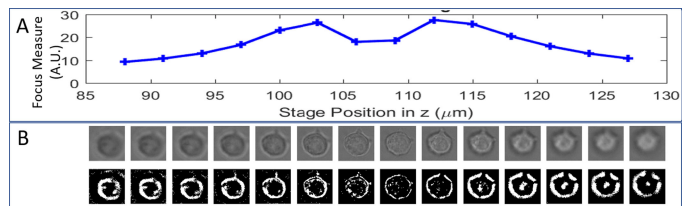


Fig. 7. (A) Focus (contrast) measure along the optical (z) axis. The focus measure increases as the focal plane approach the cell position in z, reduces at that position and increases again when the focal plane is below the cell. (B) Top: Corresponding image acquired at each position along the z axis. Bottom: The result of intensity thresholding. Pixels that are darker than the background are set to 1. The local maxima value of the measure indicates the ideal position for the stage to extract image properties of the cell.

We used the focal measure given by Equation 1 to evaluate the sharpness of the edge in each of the cell images, as shown in panel B of Fig. 7.

T cells are not adhesive cell lines. They are used directly *ex vivo* or cultured in suspension. As such, most T cells whether naive or central or effector memory T cells that would be extracted from human blood, for example, keep an almost spherical shape when touching a coated substrate. Tsang *et al* [25], for example, have shown that T cells are spherical while adhered to the surface. However, some cells elongate, which are not appropriate for the avidity test. Therefore, we do not select those elongated cells for the succeeding experimentation. Our image processing algorithm distinguishes elongated vs spherical cells by evaluating the eccentricity of each cell at 100X and selects only candidates with a low level of eccentricity and hence, circular. If T cells detach, they will move towards the center of the trap and show decoupling from sample stage movements during force application. This behaviour can be detected through visual feedback of cell and microbead positioning.

The cells were stained with a calcium indicator prior to immobilization on the cover slip. To detect elevations in calcium ions, the illuminating lamp is turned off and the cells are then excited with a 488 nm laser. The emission signal is detected with a photo diode. In general, calcium flux as a readout of early T cell activation is widely used to access the quality of TCR-pMHC specificity. There are a remarkable variety of calcium signals in T cells ranging from infrequent spikes to sustained oscillations and plateaus which can be studied.

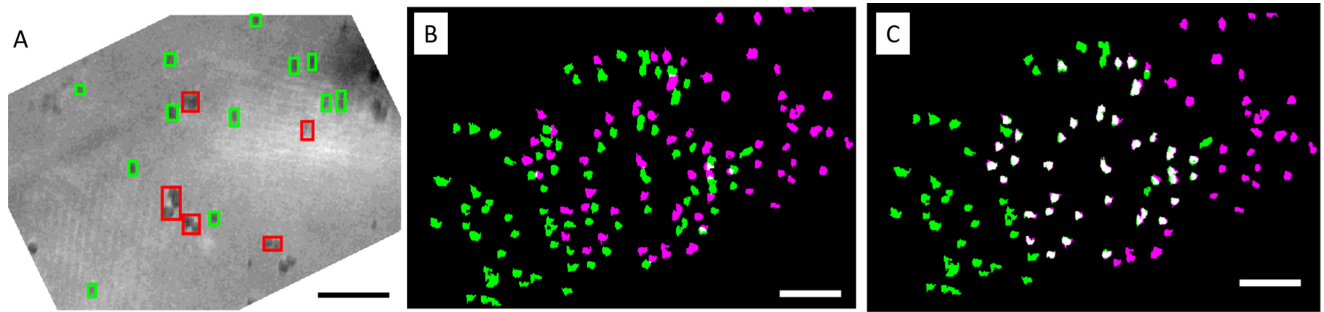


Fig. 8. (A) Image analysis results. Green boxes show single cells and red boxes show candidates with multiple cells. (B) Green blobs are extracted cells in one image. The stage is then moved translated by $60 \mu\text{m}$ in the y axis and $140 \mu\text{m}$ in the x axis and a new image is acquired. The image resolution is approximately $0.7 \mu\text{m}$ per pixel. Image in magenta shows detected cells after translating the image in the x and y based on open loop readings, which are not aligned in the original image. (C) The combined image using additional alignment techniques. Shown in white are the cells detected in both images (Scale bar: $200 \mu\text{m}$).

V. RESULTS AND DISCUSSION

Each experimental run starts with cell detection with the top camera. To detect the desired focal point, we selected a coarse step size of $150 \mu\text{m}$ above and below the current z position to determine if the focal plane for the cells is above or below. Next, we acquired an image stack at a step size of $15 \mu\text{m}$, which is slightly larger than the height of a cell, to select the best focal plane.

Fig. 8(a) shows the cell segmentation results at the selected focal plane. We can detect majority of the cells including cells which have adhered very close to each other. Approximately 88% of the cells were successfully detected in a single frame. Cells along the edges of the frame fail to be segmented due to uneven background illumination. However, by moving the stage and aligning images captured at different xy translations, the segmentation results increased to approximately 98%. Fig. 8(b) shows the blended overlay of two images, the extracted cells from the image captured prior to translating the stage (green) and the extracted cells captured after the stage is moved and translated in the x and y based on open loop readings (magenta). Fig. 8(c) shows the blended overlay after additional alignment techniques. The white blobs indicate that the same cells detected in both images are overlaid accurately.

The coordinate referencing system automatically brings cells detected in the 20X FOV to the 100X FOV. We evaluated the performance by repeating this action 20 times. The system succeeded in bringing the cells to the 100X FOV, 18 times out of 20. Our system successfully detect the bead with circular Hough transforms. In order to perform TCR acuity studies, our system adjusted the location of the cell on the axis, relative to the bead by evaluating the focus measure of the cell along the z axis and moved the stage to apply shear force to study TCR-pMHC interactions.

The interaction between TCR and pMHC results in T cell activation. This activation can be mimicked by ligation of the invariant CD3 signaling components of the TCR complex using anti-CD3 monoclonal antibody (mAb) [7]. We selected 17A2, an anti-CD3 mAb (ThermoFisher, 11-0032-80), which is conjugated with FITC molecules (a fluorescent dye). We covalently immobilize the antibody on the $3 \mu\text{m}$ protein-G coated polystyrene beads (Spherotech, PCP-30-5). To detect calcium

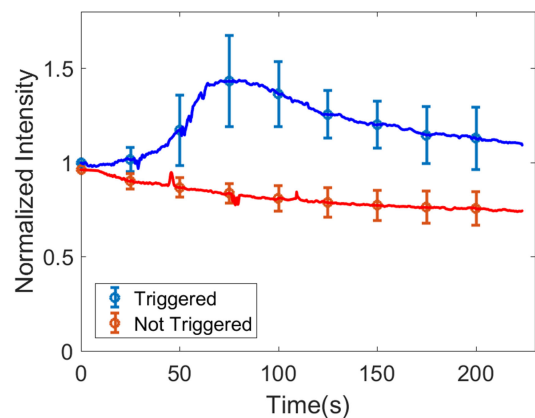


Fig. 9. Fluorescence intensity profiles detected by the avalanche photodiode for 14 different T cell acuity examinations. In seven studies, the T cells were activated (triggered). The mean and standard deviation of the triggered cases are shown in blue and while the non-triggered results are shown in red. Results show that the intensity will drop due to by photobleaching if there is no activation. However, a rise in free calcium ions results in a rise in fluorescence intensity which offsets the photobleaching effect.

signalling, our T cells were loaded with a calcium indicator (Fluo-4, ThermoFisher, F14201).

Fig. 9 shows the experimental results for T cell acuity, which is the normalized fluorescence intensity profiles over time. A total of 14 acuity tests were performed, in which 7 of them showed T cell acuity, also known as triggering (shown in blue). Shown in red is the profile when there is no activation. The error bars indicate the standard deviation of the intensity profiles. When the T cell is activated, there is a steady rise in fluorescence intensity, indicating a rise in free calcium signals. This rise, measured over time, is followed by a drop in intensity due to photobleaching.

We have provided comparing the current throughput and that of the developed methodology in Table I. When these studies are performed manually, more than half the time is occupied in finding quality cells, finding beads and calibrating (typically overall requiring 10 minutes total per cell but ranges given in Table I). In addition, the actual signalling measurement requires 5 minutes. This places the throughput for a completely manual method at 8-16 cells in a two hour slide window. Automation increases the throughput of these studies.

TABLE I
COMPARISON BETWEEN MANUAL AND AUTOMATED OPERATIONS OF TASKS
SHOW OUR SYSTEM IMPROVES EXPERIMENTAL THROUGHPUT

Task	Time	
	Manual	Automated
Detect focal plane	3-15 minutes	1 - 2 minutes
Detect T cells, Create grid coordinates	Not Performed	1 - 2 minutes
Detect and trap bead	1 - 5 minutes	1 - 5 minutes
Move a cell to trapped bead. Detect suitability	N*(2 - 5 minutes)	N*(seconds - 1 minute)
Apply shear force. Detect calcium signalling	N*(10 - 15 minutes)	N*(5 - 10 minutes)

This work substantially reduces times for finding beads, performing experiments and performing calibrations. A significant time saver with this method is the coordinate mapping so that multiple desired cells can be recovered later. The optical layout with both 100X for trapping and 20X for the larger field of view permit these tasks on the same microscope. Currently, recovery is performed on a second microscope where no more than 2-3 cells in a given field of view can be recovered.

VI. CONCLUSION

We have presented a robotic microscope system to automate highly sensitive and selective T cell activation experiments. The image-guided piezo-stage allows for fine positioning of cell-bound TCRs relative to a micron-sized bead and applying a tiny controlled force to the binding site. The image analysis algorithms automatically detect cells and beads, and quantify this activation via the fluorescence intensity. This system will be the key enabler to investigating the ability of immune cells to detect cancer cells. Future work includes integrating our system with an image-guided micropipette for capturing and recovering cells of interest for further analysis such as single cell RNA-sequencing.

REFERENCES

- [1] T. N. Schumacher and R. D. Schreiber, "Realising the promise: Neoantigens in cancer immunotherapy," *Science*, vol. 348, no. 6230, pp. 69–74, 2015.
- [2] H. T. Marshall and M. B. A. Djamgoz, "Immuno-oncology: Emerging targets and combination therapies," *Frontiers Oncol.*, vol. 8, no. August, pp. 1–29, 2018. [Online]. Available: <https://www.frontiersin.org/article/10.3389/fonc.2018.00315/full>
- [3] E. L. Reinherz, " $\alpha\beta$ TCR-mediated recognition: Relevance to tumor-antigen discovery and cancer immunotherapy," *Cancer Immunol. Res.*, vol. 3, no. 4, pp. 305–312, 2015.
- [4] Y. Feng, E. L. Reinherz, and M. J. Lang, " $\alpha\beta$ T Cell receptor mechanosensing forces out serial engagement," *Trends Immunol.*, vol. 39, no. 8, pp. 596–609, 2018. [Online]. Available: <https://doi.org/10.1016/j.it.2018.05.005>
- [5] D. K. Das *et al.*, "Force-dependent transition in the T-cell receptor β -subunit allosterically regulates peptide discrimination and pMHC bond lifetime," *Proc. Nat. Acad. Sci.*, vol. 112, no. 5, pp. 1517–1522, 2015. [Online]. Available: <http://www.pnas.org/lookup/doi/10.1073/pnas.1424829112>
- [6] D. K. Das *et al.*, "Pre-T cell receptors (Pre-TCRs) leverage $V\beta$ complementarity determining regions (CDRs) and hydrophobic patch in mechanosensing thymic self-ligands," *J. Biol. Chem.*, vol. 291, no. 49, pp. 25 292–25 305, 2016.
- [7] S. T. Kim *et al.*, "The $\alpha\beta$ T cell receptor is an anisotropic mechanosensor," *J. Biol. Chem.*, vol. 284, no. 45, pp. 31 028–31 037, 2009.
- [8] Y. Feng, K. N. Brazin, E. Kobayashi, R. J. Mallis, E. L. Reinherz, and M. J. Lang, "Mechanosensing drives acuity of $\alpha\beta$ T-cell recognition," *Proc. Nat. Acad. Sci.*, vol. 114, pp. E8204–E8213, 2017. [Online]. Available: <http://www.pnas.org/lookup/doi/10.1073/pnas.1703559114>
- [9] X. Wang *et al.*, "A three-dimensional magnetic tweezer system for intra-embryonic navigation and measurement," *IEEE Trans. Robot.*, vol. 34, no. 1, pp. 240–247, Feb. 2018.
- [10] E. Shojaei-baghini and Y. Sun, "Robotic micropipette aspiration of biological cells," *Exp. Robot.*, vol. 109, pp. 591–602, 2016. [Online]. Available: <http://link.springer.com/10.1007/978-3-319-23778-7>
- [11] L. Yang, I. Paranaewithana, K. Youcef-Toumi, and U. X. Tan, "Automatic vision-guided micromanipulation for versatile deployment and portable setup," *IEEE Trans. Automat. Sci. Eng.*, vol. 15, no. 4, pp. 1609–1620, Dec. 2017.
- [12] Z. Lu, C. Moraes, G. Ye, C. A. Simmons, and Y. Sun, "Single cell deposition and patterning with a robotic system," *PLoS One*, vol. 5, no. 10, p. e13542, 2010.
- [13] J. Liu *et al.*, "Automated robotic measurement of 3-D cell morphologies," *IEEE Robot. Automat. Lett.*, vol. 2, no. 2, pp. 499–505, Apr. 2017. [Online]. Available: <http://ieeexplore.ieee.org/document/7797448/>
- [14] A. Ranaweera and B. Bamieh, "Modelling, identification, and control of a spherical particle trapped in an optical tweezer," *Int. J. Robust Nonlinear Control*, vol. 15, no. 16, pp. 747–768, 2005.
- [15] C. Aguilar-Ibanez, M. S. Suarez-Castanon, and L. I. Rosas-Soriano, "A simple control scheme for the manipulation of a particle by means of optical tweezers," *Int. J. Robust. Nonlinear Control*, vol. 21, pp. 328–337, 2011.
- [16] Q. M. Ta and C. C. Cheah, "Simultaneous orientation and positioning control of a microscopic object using robotic tweezers," in *Proc. IEEE Int. Conf. Robot. Automat.*, 2017, pp. 5864–5869.
- [17] Q. M. Ta and C. C. Cheah, "Stochastic control for optical manipulation of multiple microscopic objects," *Automatica*, vol. 89, pp. 52–64, 2018. [Online]. Available: <https://doi.org/10.1016/j.automatica.2017.11.031>
- [18] C. C. Cheah, X. Li, X. Yan, and D. Sun, "Observer-based optical manipulation of biological cells with robotic tweezers," *IEEE Trans. Robot.*, vol. 30, no. 1, pp. 68–80, Feb. 2014.
- [19] X. Li, C. C. Cheah, X. Yan, and D. Sun, "Robotic cell manipulation using optical tweezers with limited FOV," in *Proc. IEEE Int. Conf. Robot. Automat.*, 2014, pp. 4588–4593.
- [20] E. B. Steager, B. Zern, M. S. Sakar, V. Muzykantov, and V. Kumar, "Assessment of protein binding with magnetic microrobots in fluid," in *Proc. IEEE Int. Conf. Robot. Automat.*, 2013, pp. 5502–5507.
- [21] Y. Cong *et al.*, "Mass spectrometry-based monitoring of millisecond protein–ligand binding dynamics using an automated microfluidic platform," *Lab Chip*, vol. 16, no. 9, pp. 1544–1548, 2016.
- [22] A. K. Khitrin, J. C. Petrucci, and M. A. Model, "Bright-field microscopy of transparent objects: A ray tracing approach," *Microsc. Microanal.*, vol. 23, no. 6, pp. 1116–1120, 2017.
- [23] M. R. B. Alberts, A. Johnson, J. Lewis, D. Morgan, K. Roberts, and P. Walter, *Molecular Biology of the Cell*, 6th ed. Mark L. Richter, Ed. New York, NY, USA: Garland Science, 2014.
- [24] J. M. Geusebroek, F. Cornelissen, A. W. Smeulders, and H. Geerts, "Robust autofocusing in microscopy," *Cytometry*, vol. 39, no. 1, pp. 1–9, 2000.
- [25] M. Tsang, J. Gantchev, F. M. Ghazawi, and I. V. Litvinov, "Protocol for adhesion and immunostaining of lymphocytes and other non-adherent cells in culture," *BioTechniques*, vol. 63, no. 5, pp. 230–233, 2017.